Supporting information

Experimental Section

Sample preparation and characterization: Ultrathin SnS_2 nanosheets were synthetized via CVD in a horizontal vacuum furnace tube. To grow SnS_2 nanosheets, Sn granules (1 g, Aldrich) were placed in a quartz boat at the center of furnace, and sulfur powder (0.8 g, Aldrich) was placed in another quartz boat upstream in the furnace. Segments of a 300 nm SiO_2/Si wafer were placed face up in a quartz boat downstream of the sources. Prior to growth, the tube was cleaned by high-purity Ar at a rate of 300 standard cubic centimeter per minute (sccm) for 10 minutes to eliminate oxygen in the furnace. After flushing the tube with high-purity Ar three times and pumping to 30 mtorr, the furnace was heated to 700 ℃ in 20 minutes and kept at this temperature for 45 minutes. During the growth process, high-purity Ar with a flow rate of 60 sccm was used as the carrier gas. Finally, the furnace was naturally cooled to room temperature and the ultrathin SnS_2 nanosheets formed on the 300 nm SiO_2/Si substrates were recovered. The optical images and SEM images of SnS_2 were obtained using a Shanghai 9XB-PC microscope and SEM (Cari Zeiss). The thicknesses were measured using Seiko SPI3800N AFM. The Raman spectra of the synthesized SnS_2 were measured using Renishaw 2000 confocal Raman system. The crystal structural characterization was performed by transmission electron microscope

(TEM, JEOL-TEM).

Device fabrication and measurements: SnS_2-based devices were fabricated using UV lithography and silver wires shadow mask methods, and Ti/Au (10 nm/100 nm) metal electrodes were deposited by electron beam evaporation. The electronics, optoelectronics and gas sensing data were collected using a Keithley 2400. Several Laser diodes were used as light sources for measurements of the light response under ambient conditions. To measure the gas response, the SnS_2-based gas sensors were sealed in a transparent chamber and partial flows NO_2 and N_2 gas were alternately introduced, with a total flow velocity 200 sccm. Before each measurement, the chamber was pumped to a vacuum state for more than 1 hour to desorb contaminant molecules and regenerate the surface, then pure dry N_2 was injected for more than 1 hour to stabilize the original state for NO_2 testing in a N_2 background. The pressure of chamber was kept at standard atmospheric pressure.

DFT simulation:

Calculations of the electronic structure of a SnS_2 monolayer with an adsorbed NO_2 molecule was performed using the density functional theory (DFT) implemented in the VASP package[1, 2]. The VASP package utilizes the projector augmented wave (PAW) method. The exchange and correlation energies used the Perdew-Burke-Ernzerhof (PBE) functional with the generalized gradient approximation (GGA)[1, 2].The energy cutoff for the plane-wave basis expansion was set to 350 eV and an energy convergence criteria of 1×10^{-5} eV per unit cell was chosen. A $12\times12\times1$ k-grid mesh was used to sample the Brillouin zone. Initially, we used the experimental lattice parameters of bulk SnS_2[3] to construct the SnS_2 monolayer. We fixed the in-plane lattice constant and optimized all the atoms in the supercell. The residual force and stress were less than 0.01 eV/A and 1.0 kBar, respectively. The vacuum thickness of supercell was above 15Å. For the SnS_2 adsorption of a NO_2 molecule, the van der Waals force correction[4] was adopted to optimize the lattice structural parameters and bond length. The spin polarization calculation also was adopted to calculate the binding energy and electrical conductivity, due to the NO_2 is polar molecule. We constructed a 3X3X1 SnS_2 monolayer supercell to connect with a NO_2 molecule, of the type Sn_9S_{18} which contend 9 Sn atoms and 18 S atoms. Also, another 3X3X1 SnS_2 monolayer supercell with one S vacancy named of the stoichiometrySn_9S_{17}. The adsorption energy calculation result is based on the above described supercell. The N-O bonds point down to the SnS_2 monolayer which implies the O atom is located between the N and S atoms. For brevity, in the present study, we only calculated the N-O bonds pointing down towards the SnS_2 monolayer shown in Fig. 7(a). The electron conductivity was calculated as a function of the chemical potential μ for the temperature T = 300K. All of the calculation results were obtained by the wannier90 code within BoltzWann module[5, 6]. Initially, starting the 12x12x1 grid for the construction of the Wannier function and using the dense 80x80x1 mesh to calculate the BoltzWann module. The VESTA package was used to draw the charge density difference of SnS_2 monolayer adsorbing a NO_2 molecule, and with S vacancy[7].

Formula 1

The calculation of mobility

we can estimate the mobility of the SnS_2 using the following equation:

$$\mu = \frac{dI_{DS}}{dV_G} \cdot \frac{L}{WC_{SiO_2}V_{DS}}$$

where L=45.5 μm and W=32.7 μm are the length and width of the conduction channel, respectively, and $C_{SiO2} = \varepsilon_0\varepsilon_r/d$ is capacitance per unit area estimated for the gate dielectric, with ε_0 being the free-space permittivity, ε_r=3.9 is the relative permittivity for SiO_2, and d=300 nm is the thickness of the SiO_2. The calculated C_{SiO2} for 300 nm thick SiO_2 is ≈1.6 nF/cm^2 and the calculated mobility is μ=9.7 cm^2/Vs.

Formula 2

The calculation of responsivity and external quantum efficiency

The responsivity (R_λ) and external quantum efficiency (EQE) can be calculated by the following relationships:

$$R_\lambda = I_{ph}/PS$$

$$EQE = hcR_\lambda/e\lambda$$

where $I_{ph} = I_{photo} - I_{dark}$=1.38 μA is the photocurrent, I_{photo} and I_{dark} are the currents with and without laser illumination, *P* is the incident light intensity, *S*=1488 μm^2 is the effective illuminated area, *h* is Planck's constant, *e* is the electronic charge and λ= 532 nm is the wavelength of incident light. Thus, R_λ and the EQE of our device are 31 AW^{-1} and 7.7×10^3 %, respectively.

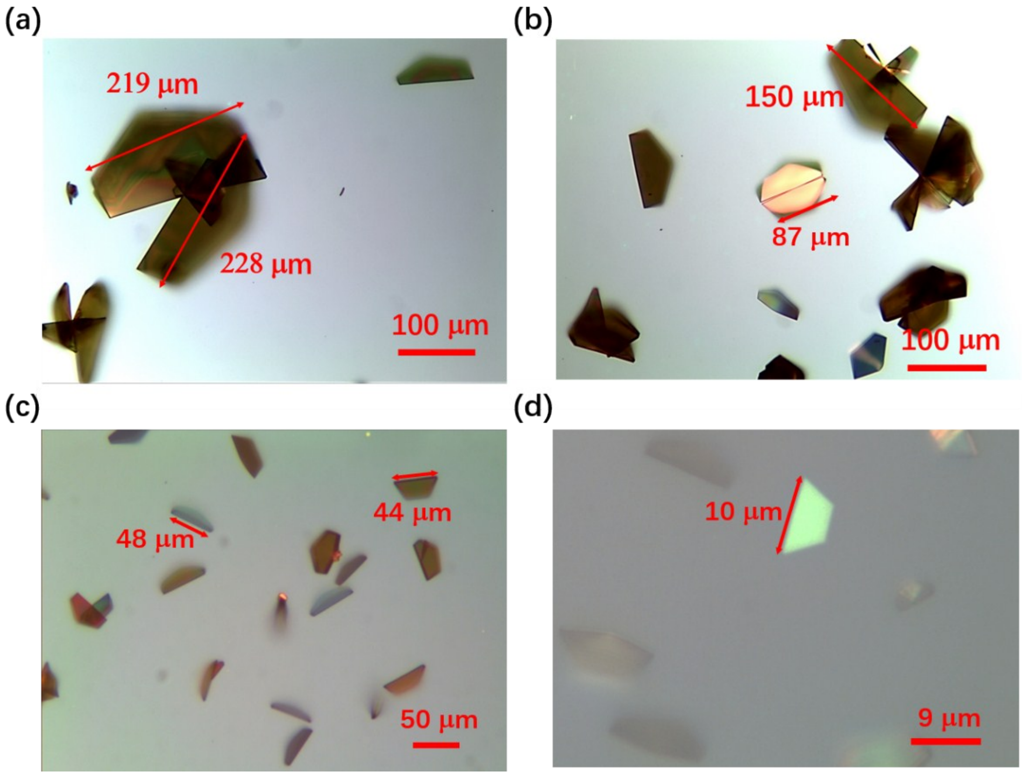

Figure S1： Optical images of semi-hexagonal SnS_2 nanosheets with different lateral dimensions.

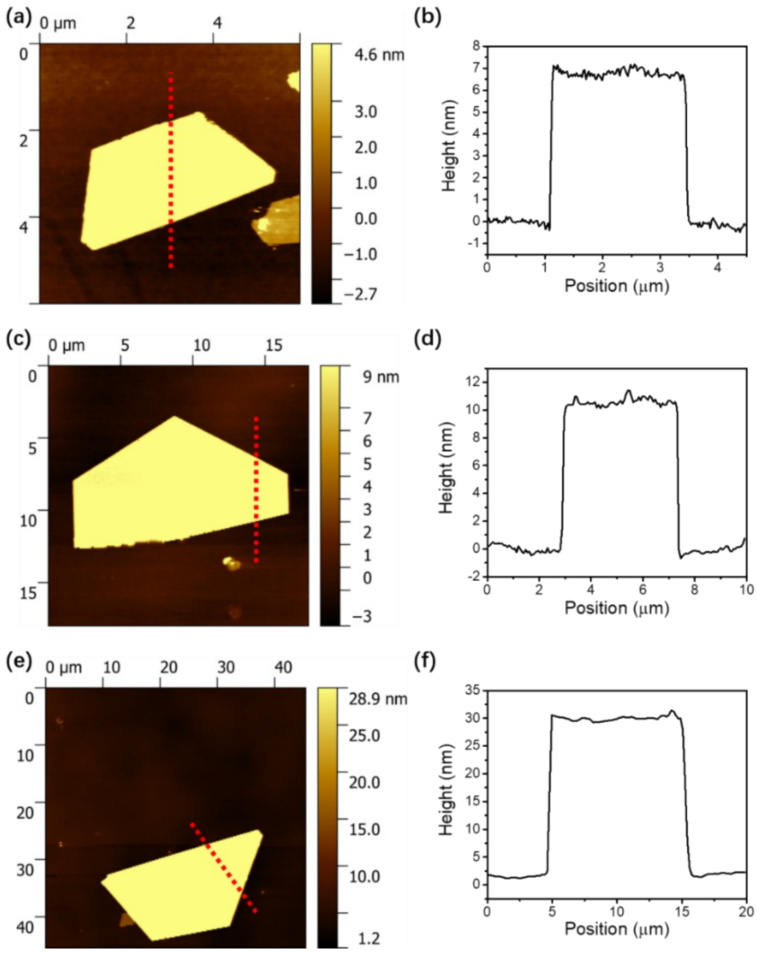

Figure S2: (a, c, e) Three examples of AFM images of semi-hexagonal SnS_2 nanosheets. (b, d, f) Corresponding height profiles of the dashed line shown in (a, c, e).

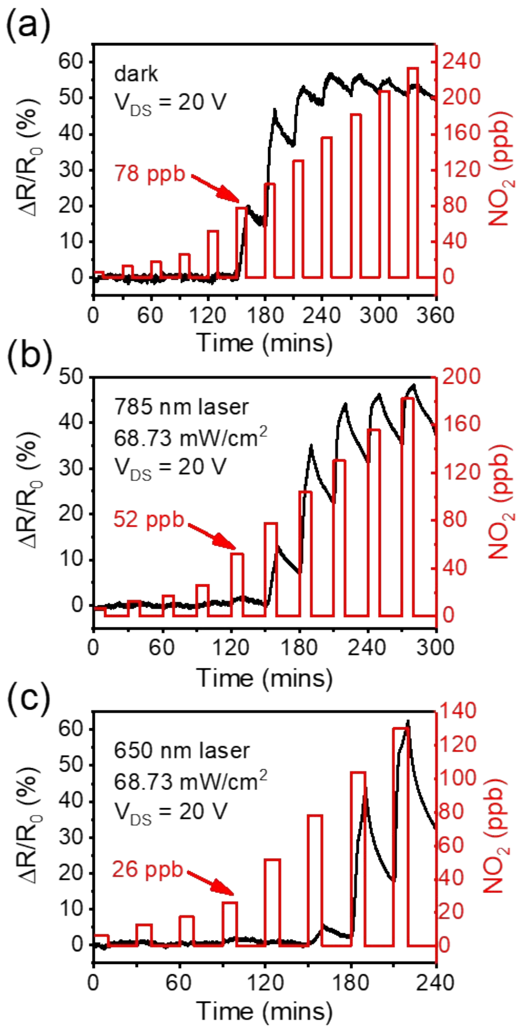

Figure S3: Dynamic sensing response of $^{\Delta R}/_{R_0}$ change versus time for the SnS_2-based sensor upon exposure to NO_2 gas with concentrations ranging from 6.5 ppb to 130 ppb in the dark (a) and under 785 nm (b) and 650 nm (c) laser irradiation.

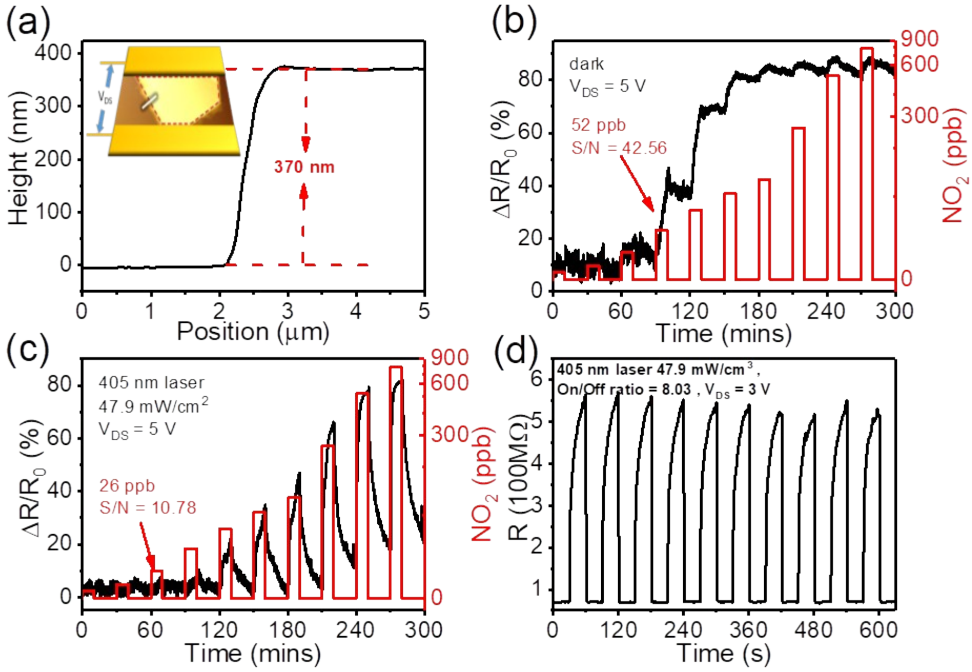

Figure S4. (a) Height profile of SnS_2 sample-1 along the white line in the inset AFM image. Dynamic sensing response of $\Delta R/R_0$ change versus time for the sensor upon exposure to NO_2 gas with different concentrations under (b) dark environment and (c) 405 nm laser irradiation. (d) The time-resolved photon response measured with on/off ratio of 8.

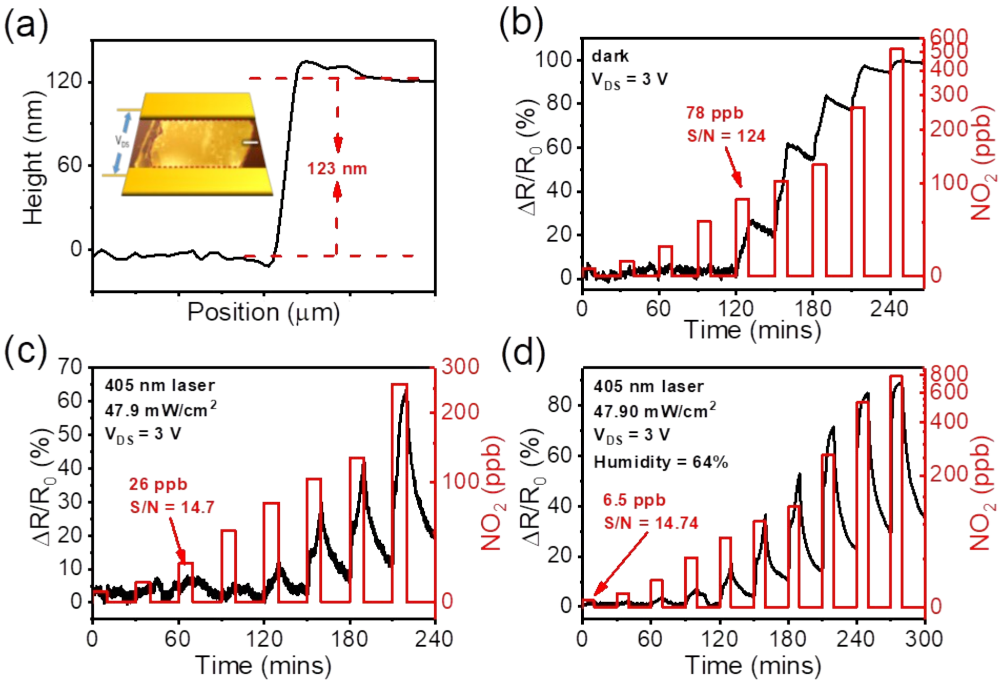

Figure S5. (a) Height profile of SnS_2 sample-2 along the white line in the inset AFM image. Dynamic sensing response of $\Delta R/R_0$ change versus time for the sensor upon exposure to NO_2 gas with different concentrations under (b) dark environment, (c) 405 nm laser irradiation and (d) 64% humidity with 405 nm laser irradiation.

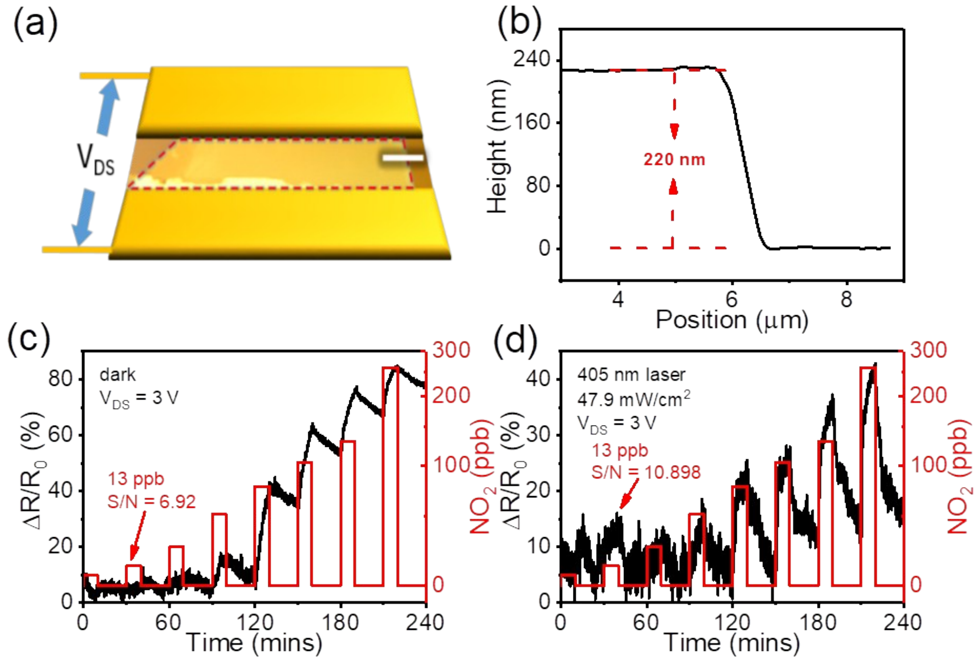

Figure S6. (a) The AFM image of SnS_2 sample-3. Corresponding to the white line in (a), the height profile was showed in (b). Dynamic sensing response of $\Delta R/R_0$ change versus time for the sensor upon exposure to NO_2 gas with different concentrations under (c) dark environment and (d) 405 nm laser irradiation.

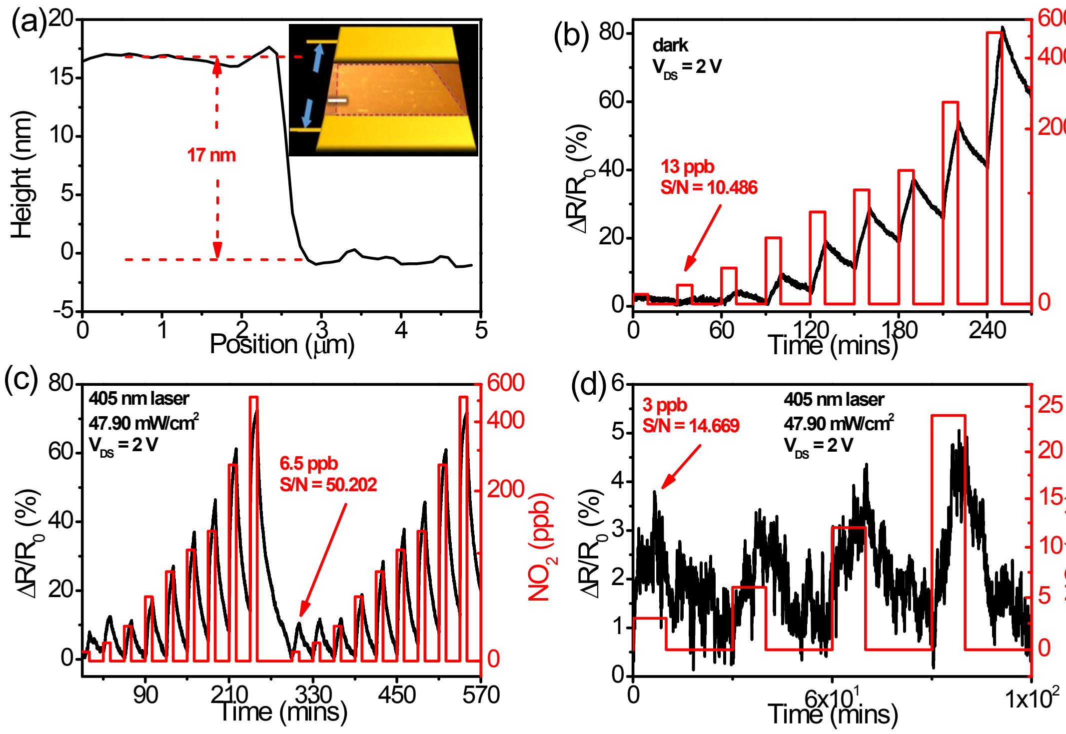

Figure S7. (a) Height profile of SnS_2 sample-4 along the white line in the inset AFM image. Dynamic sensing response of $\Delta R/R_0$ change versus time for the sensor upon exposure to NO_2 gas with different concentrations under (b) dark environment and (c, d) 405 nm laser irradiation. (c) A stability test of repeating NO_2 concentration changing from 6.5 to 580ppb for two times.

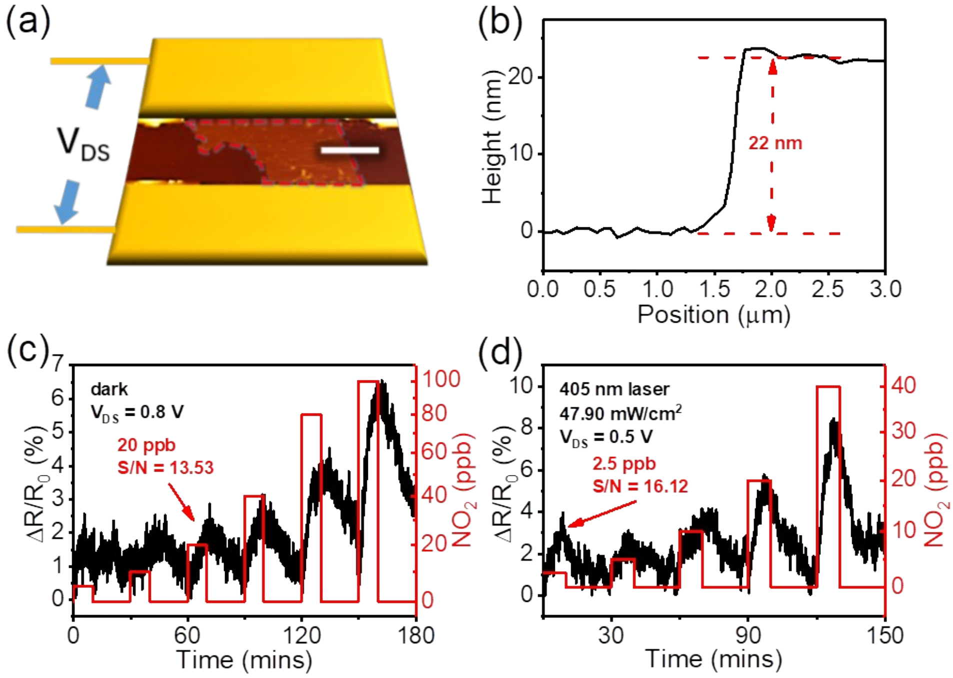

Figure S8. (a) The AFM image of SnS_2 sample-5. Corresponding to the white line in (a), the height profile was showed in (b). Dynamic sensing response of $\Delta R/R_0$ change versus time for the SnS_2 sample-6 sensor upon exposure to NO_2 gas with different concentrations under (c) dark environment and (d) 405 nm laser irradiation.

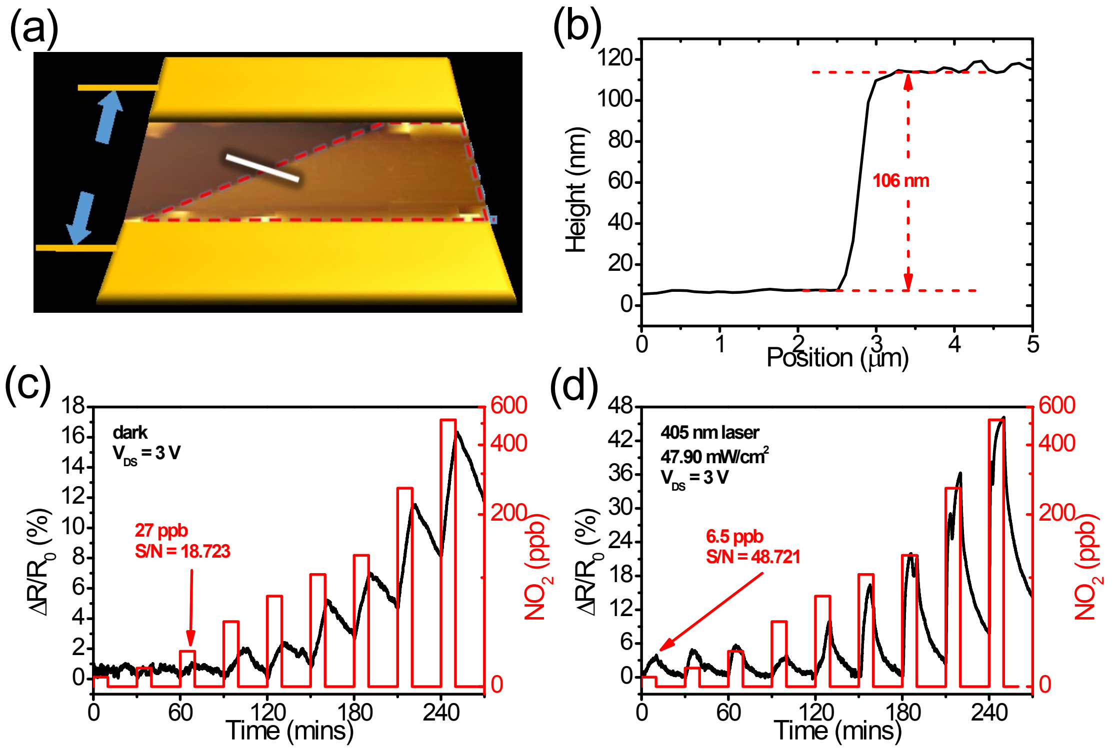

Figure S9. (a) The AFM image of SnS_2 sample-6. Corresponding to the white line in (a), the height profile was showed in (b). Dynamic sensing response of $\Delta R/R_0$ change versus time for the sensor upon exposure to NO_2 gas with different concentrations under (c) dark environment and (d) 405 nm laser irradiation.

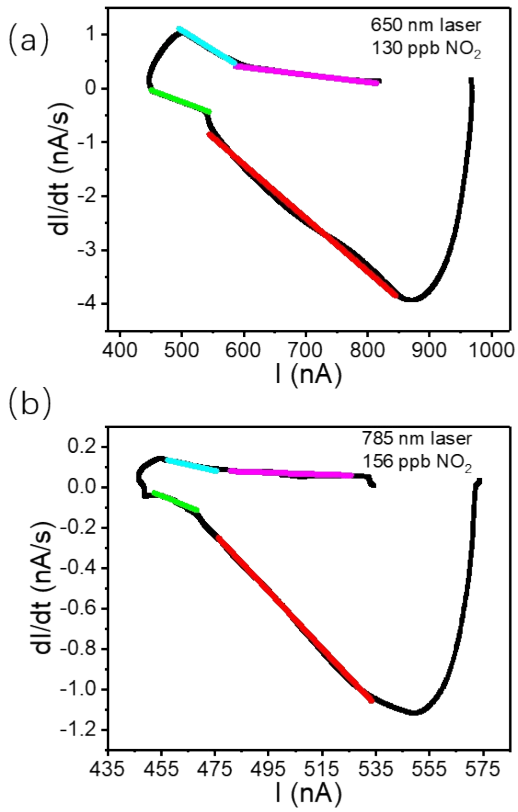

Figure S10. (a) The dI/dt-I curve of 130 ppb NO_2 test under 650 nm laser illumination. (b) The dI/dt-I curve of 156ppb NO_2 test under 785 nm laser illumination.

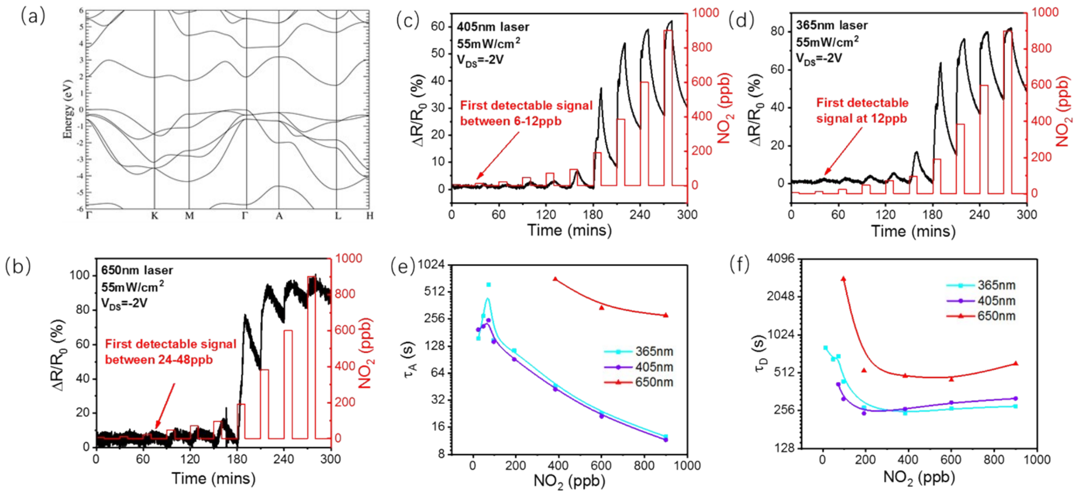

Figure S11. (a) Calculated band structure of SnS_2. Gas sensing performance of another sensor under (b) 365 nm, (c) 405 nm, and (d) 650 nm laser illuminations. (e) Absorption time and (f) desorption time as a function of gas concentration.

Reference:

[1] G. Kresse, J. Furthmüller, *Computational Materials Science*. **1996**, 6, 15.

[2] G. Kresse, J. Furthmüller, *Physical Review B*. **1996**, 54, 11169.

[3] R. M. H. A. L. W. FINGER, *Journal of the Ceramic Association Japan*. **1978**, 63, 293.

[4] S. Grimme, *J. Comput. Chem.* **2006**, 27, 1787.

[5] A. A. Mostofi, J. R. Yates, G. Pizzi, Y.-S. Lee, I. Souza, D. Vanderbilt, N. Marzari, *Comput. Phys. Commun.* **2014**, 185, 2309.

[6] G. Pizzi, D. Volja, B. Kozinsky, M. Fornari, N. Marzari, *Comput. Phys. Commun.* **2014**, 185, 422.

[7] K. Momma and F. Izumi, J. Appl. Crystallogr. **2011**, 44, 1272-1276.